CONFIDENTIAL

COPY NO. 21

NATIONAL AERONAUTICAL ESTABLISHMENT
CANADA

LABORATORY REPORT LR-116

THE AERODYNAMIC CHARACTERISTICS OF A TAIL-FIRST DELTA WING CONFIGURATION AT M = 1.57

BY

J. A. VAN DER BLIEK AND J. D. STEWART

OTTAWA

29 OCTOBER 1954

NATIONAL AERONAUTICAL ESTABLISHMENT

Canada

LABORATORY REPORT

Aerodynamics Laboratory

Pages - Preface - 6
Text - 15
Figures - 23

CONFIDENTIAL
Laboratory Report: LR-116
Date: 29 October 1954
Lab. Order: 9654A
File: CM49-7-16

For: Internal

Subject: THE AERODYNAMIC CHARACTERISTICS OF A TAIL-FIRST DELTA WING CONFIGURATION AT M = 1.57.

Prepared by: J.A. van der Bliek
J.D. Stewart

Submitted by: J. Lukasiewicz
Head
High Speed Aerodynamics Laboratory

R.J. Templin
Acting Head
Aerodynamics Section

Approved by: J.H. Parkin
Director

SUMMARY

The aerodynamic characteristics of a tail-first type half-model having an aspect ratio 2.12 delta wing were obtained in the N.A.E. 30-inch wind tunnel at a Mach number

of 1.57 and a Reynolds number of 2.2 million, based on the wing mean aerodynamic chord.

The results were obtained for both a high-wing and a low-wing configuration at angles of attack from -6 degrees to +12 degrees. The tail setting was varied in 2-degree increments from -4 degrees to +10 degrees, also the tail-off configuration was tested. Separate tests were carried out on the body alone, with and without tail fairing and on a similar N.A.C.A. fuselage, to determine the effect on drag of the tail fairing.

The results showed that for the centre of gravity location considered, the forward tail could balance the aircraft up to lift coefficients of about 0.7 for the low wing configuration and up to 0.4 for the high wing configuration. However, the static margin was such that the model would have been probably unstable subsonically. In general, the low wing configuration was more efficient than the high wing one.

The performance of the tail-first model was compared with that of similar delta wing models fitted with trailing-edge controls.

TABLE OF CONTENTS

List of Illustrations

List of Illustrations (Cont'd)

LIST OF SYMBOLS

A	$= \frac{2b_1^2}{S}$ = aspect ratio
b_1	wing semi-span, inch
$\bar{c}$	mean aerodynamic chord, inch
C_L	$= \frac{L}{qS}$ = lift coefficient
C_{L_α}	lift curve slope at zero lift, per degree
$(C_L)_{(L/D)_{max.}}$	$= \sqrt{C_{D_o}\pi Ae}$ = lift coefficient for $(L/D)_{max.}$
C_m	pitching moment/$qS\bar{c}$ = pitching moment coefficient about the 30.9 percent chord point of the mean aerodynamic chord, unless stated otherwise
$\left(\frac{dC_m}{dC_L}\right)_{C_L=0}$	static longitudinal stability parameter at zero lift
$\frac{dC_m}{di_T}$	pitching moment control effectiveness parameter, per degree
C_D	$= \frac{D}{qS}$ = drag coefficient
C_{D_o}	drag coefficient at zero lift, based on wing area unless stated otherwise
C_{p_B}	$= \frac{pB-p}{q}$ = base pressure coefficient
e	$= \frac{dC_L^2}{dC_D}\Big/\pi A$ = wing span efficiency factor
i_T	tail incidence angle (nose up positive), degrees
$(L/D)_{max.}$	$= \sqrt{\frac{\pi Ae}{4C_{D_o}}}$ = maximum lift-drag ratio

LIST OF SYMBOLS (CONT'D)

M	Mach number
p	free stream static pressure, p.s.i.
p_B	pressure at model base, p.s.i.
q	dynamic pressure, p.s.i.
Re	Reynolds number based on the mean aerodynamic chord, unless stated otherwise
S	semi-span gross wing area, inch^2
α	angle of attack, degrees
α_B	angle of attack at breakpoint of lift curve, degrees
$\alpha_{L=0}$	angle of attack at zero lift, degrees
δ_e	flap angle measured perpendicular to hinge line (flap down positive), degrees

THE AERODYNAMIC CHARACTERISTICS OF A TAIL-FIRST DELTA WING CONFIGURATION AT M = 1.57

1. INTRODUCTION

As part of a program instituted to study the performance of longitudinal control surfaces for a supersonic aircraft, a tail-first model was tested in the N.A.E. High-Speed Aerodynamics Laboratory 30-inch wind tunnel at a Mach number of 1.57 and a Reynolds number of 2.2 million based on the mean aerodynamic chord. The present results are concerned with the aerodynamic characteristics of an aspect ratio 2.12 delta wing model with the model considered as both a high wing and a low wing aircraft.

The effects of the tail on the wing were investigated by testing the wing-body configuration alone.

Because of the high value of C_{D_o} compared with similar data on a trailing edge flap controlled model the body alone was tested with and without the tail fairing. Also the fuselage of identical shape as that utilized in a model with trailing edge flap was tested in the 30-inch wind tunnel.

2. WIND TUNNEL, MODEL MOUNTING, FORCE AND PRESSURE MEASUREMENTS

The half-model tests were conducted in the 30 x 16 inch tunnel at a Mach number of 1.57, using a fixed magnesium nozzle liner. The Mach number distribution in the region of the model was uniform to better than 1 percent.

The tunnel used dry air with a specific humidity of less than 0.0005 at approximately room temperature and atmospheric stagnation pressure.

The half-model, as attached to the balance, was displaced 0.28 inch from the tunnel wall, on which a 0.25-inch shim was mounted. Thus a gap of approximately 0.03 inch existed between the model and the shim. Although the shim was mounted independently of the model, it rotated with it through the various incidences.

The normal force, chord force and pitching moment were measured on a three-component strain gauge balance with

the outputs being recorded by high speed self-balancing potentiometers. The recorders were provided with adjustable sensitivity which permitted reading accuracies up to ±0.2 percent. The base pressure was measured with an electrical pressure transducer. The output of the pressure transducer was recorded in the same way as the balance outputs.

3. TEST MODEL

A three view drawing of the model is shown in Figure 1 and photographs of the model installed in the wind tunnel are given in Figures 2 and 3. The main dimensions of the model are given in Figure 1 and the other geometric properties are given in Table I below.

TABLE I MODEL DATA

Wing aerofoil section parallel to the plane of symmetry	N.A.C.A. 0003-63
Half wing gross area	$S = 23.34$ in.^{2}
Wing mean aerodynamic chord	$\bar{c} = 6.01$ in.
Wing aspect ratio	$A = 2.12$
Wing taper ratio	$\tau = 0.04$
Wing dihedral	0°
Wing incidence	0°
Wing geometric twist	0°
Wing leading edge sweep back angle	$\Lambda = 60°$

TABLE I (CONT'D)

Tail aerofoil section	N.A.C.A. 0003-63
Half tail gross area	S_t = 4.38 in.^{2}
Tail aspect ratio	A_t = 2.12
Tail taper ratio	τ = 0.04
Tail dihedral	0°
Tail leading edge sweepback	Λ = 60°
Maximum half-body frontal area	0.925 in.^{2}
Ratio of gross tail area to gross wing area	$\frac{S_t}{S}$ = 0.1875
Ratio of maximum body frontal area to gross wing area	0.0396
Body fineness ratio based on actual body length	10.3

The coordinates of the aerofoil section and the fuselage without the tail fairing are given in Tables II and III respectively.

The model was constructed of solid steel and was given a protective flash coating of copper. The tail incidences could be varied from -10 degrees to +10 degrees in 2 degree increments. The tail pivoted about the 66 percent chord point of its mean aerodynamic chord. No gap existed between the tail and the body profile at any of the tail settings investigated.

TABLE II	
Aerofoil Section NACA 0003-63	
x/c%	±y/c%
0	0
1.25	0.475
2.50	0.654
5.00	0.889
7.50	1.050
10.00	1.171
15.00	1.337
20.00	1.435
25.00	1.486
30.00	1.501
40.00	1.451
50.00	1.324
60.00	1.141
70.00	0.916
80.00	0.656
90.00	0.362
95.00	0.202
100.00	0.032

TABLE III	
Fuselage Diameters	
x(in.)	2r(in.)
0.000	0.000
0.438	0.222
0.882	0.408
1.758	0.708
3.516	1.104
5.280	1.344
7.032	1.536
8.808	1.536
10.560	1.536
12.330	1.536
13.200	1.500
14.088	1.374
14.952	1.146
15.408	0.972
15.858	0.750
17.000	0.000

4. TEST PROCEDURE

The model was tested at nominal angles of attack from -6 degrees to +12 degrees with the tail setting fixed. The procedure was repeated for each tail setting from -4 degrees to +10 degrees at 2 degree increments for both high wing and low wing configurations. The normal force, chord force and pitching moment were recorded at each angle of attack.

The uncertainties in obtaining the various parameters are given in the following table.

TABLE IV	
Quantity	Uncertainty
Lift coefficient	± 0.003 at C_{L_o} up to ± 0.017 at high angles of attack
Drag coefficient	± 0.0012 at C_{D_o} up to ± 0.005 at high angles of attack
Pitching moment coefficient	± 0.00065 up to ± 0.0011 at high angles of attack
Mach number	$\pm .005$
Angle of attack	$\pm .05°$*)
Tail incidence	$\pm .05°$

*) Not included the angle of flow variation. From pressure measurements along the tunnel wall the maximum angle of flow variation was estimated at $\pm 0.15°$.

The base pressure of the model was measured at a nominal angle of attack of 0 degrees for the tail-off configuration with a probe located in the model horizontal centreline and about 3/8 inch from the tunnel wall. The probe was constructed of 0.042 inch outside diameter and 0.031 inch inside diameter stainless steel tubing. A gap of about 1/8 inch existed between the model base and the probe (see Fig. 3).

It was found from repeats of tests that the values of the so determined base pressure coefficient were not consistent. Therefore another method of measuring the base pressure was used in the tests on the half-bodies. This was

particularly necessary because the base drag on these bodies represented a much larger part of the total drag. The method used on the half-bodies of revolution is illustrated in Figure 4. By extending the brass tube with pieces of plastic tubing, the base pressure was determined at different positions of the base.

5. RESULTS

In this report only typical curves are shown for the purpose of analysis. The basic aerodynamic characteristics for the low and high wing configurations are shown in Figures 6 and 8. The data for the two configurations with the tail removed are shown in Figures 7 and 8.

The data for the high wing configuration were obtained by reading the angles of attack and tail incidence opposite to the ones read for the low wing model.

The base pressure coefficient was $C_{p_B} = -0.0685$. This corresponded to a drag coefficient $C_D = 0.0006$, based on wing area. This very low value was neglected in determining the drag coefficient.

For the high and low wing configurations the zero lift drag (Fig. 11) had a minimum value at zero tail incidence and attained substantially same values at corresponding angles of tail incidence.

With the tail removed the minimum drag was the same as for the tail-on configuration, with the tail at zero incidence, indicating a negligible tail drag. The contribution of the tail to C_{D_o} (at zero tail incidence) as estimated from wing alone tests (Ref. 1) was 0.00055. This amounts to 3.2 percent of C_{D_o}, being within the error of the measurement of C_{D_o}.

The lift curves for the low wing configuration (Fig. 6) were linear throughout the angle of tail incidence range, except at the largest tail incidence (+10 degrees). Changing the tail incidence had a negligible effect on the lift curve slope (Fig. 12), but resulted in a small shift in angle of attack for zero lift (Fig. 14).

For the high wing configuration, however, the lift curve consisted of two straight line segments (Fig. 6). This break in the lift curve occurred at different angles of attack (α_B) as the angle of tail incidence was changed (see Fig. 13). This effect may have been due to the interaction of the wave from the trailing edge of the tail surface with the wing leading edge. The lift curve slope decreased with increasing angle of tail incidence (Fig. 12) and was less than for the low wing configuration. Thus, there was an interference effect between the tail and the wing for the high wing configuration.

For the tail-off configuration (Fig. 7) the lift curve was linear at lower angles of attack. The lift curve slope (Fig. 12) was reduced by 0.0015 per degree for the low wing configuration.

Previous tests of the wing alone (Ref. 1) at a Mach number of 1.57 gave a lift curve slope of 0.0377 per degree compared with the 0.04 and 0.0415 values for the high and low wing-body configurations respectively (Fig. 12).

The pitching moment curves for the low and high wing and tail-off configurations (Fig. 8) were non-linear over the entire angle of attack range. However the curve for the wing alone was linear over the angle of attack range here considered (see Ref. 1).

For the low wing configuration, the static margin decreased with increasing tail angle (Fig. 15), giving a maximum static margin of about 6.5 percent at zero tail incidence. With increasing angle of attack the static margin was decreased and was approaching neutral stability at lift coefficients of about 0.6.

For the high wing configuration, the static margin was slightly increasing with increasing tail incidence (Fig. 15) and angle of attack.

For the tail-off configuration the centre of pressure was moved downstream, but static margin was still less than for the wing alone (Ref. 1), indicating a destabilizing effect of the fuselage.

The low static stability margin with tail on indicated that a similar aircraft configuration probably would have been unstable at subsonic speeds.

The drag due to lift curves (Fig. 10) for the low and high wing configurations consisted of two straight line segments for the low angles of attack. The slopes of the curves were different at positive and negative lift coefficients. As the tail incidence was increased (positively or negatively) this discontinuity became more pronounced. For the low wing configuration the span efficiency for the negative lift condition at negative angles of attack was less than for the positive lift condition and the reverse was true for positive tail incidences. Opposite effects appeared with the high wing model.

Only the positive lift conditions have been considered in the determination of the span efficiencies and the maximum lift-drag ratios. The span efficiency for the low wing configuration decreases as the tail incidence increases positively or negatively (Fig. 18) having a maximum value at about -2 degree tail incidence. Removing the tail had only a small effect on the span efficiency. For the high wing configuration the span efficiency decreased with increasing tail incidence. Removing the tail produced an increase in span efficiency. For the wing alone (Ref. 1) the span efficiency was almost the same as for the model considered here.

The maximum lift-drag ratio was determined from the slope of the drag due to lift curve and the minimum drag obtained from the polar curves. The maximum lift-drag ratio decreased as the absolute tail incidence was increased. Removal of the tail had little effect (Fig. 19). However, the maximum lift drag ratio for the wing alone (Ref. 1) was about 70 percent larger.

The lift coefficient for the maximum lift-drag ratio increased as the tail setting angle was increased, with negligible effects due to removal of the tail (Fig. 20). The lift coefficient for maximum lift-drag ratio was much higher for the low and high wing configuration than for the wing alone.

The curve of tail incidence versus lift coefficient for trim conditions for the low wing configuration (Fig. 17) was non-linear through the range considered. Tail incidences up to 10 degrees could trim the aircraft up to lift coefficients of 0.7. For the high wing aircraft model this curve consisted of two straight lines (Fig. 17). The required angles of tail incidence were in general much larger than for the low wing configuration.

The curves of pitching moment coefficient versus tail setting for constant C_L were linear for the lower tail settings only (Fig. 9). The pitching moment control effectiveness parameter dC_m/di_T decreased as the lift coefficient was increased positively or negatively (Fig. 16) for the low wing configuration. For the high wing configuration the control effectiveness at positive lift coefficients was much smaller.

6. COMPARISON OF TAIL-FIRST MODEL WITH A TRAILING EDGE CONTROL SURFACE MODEL

The present low wing data have been compared with those obtained with a mid-wing half model using a delta wing with a 25 percent constant percent chord flap. Figure [illegible] the main dimensions of this model. The other geometric [illegible] are summarized in Table V. For comparison the figures [illegible] the tail first model are also given in Table V.

TABLE V MODEL DATA

	Tail-first Model	Flap control Model
Wing aerofoil section parallel to the plane of symmetry	NACA 0003-63	NACA 0003-63
Half wing gross area	$S = 23.34$ in.^{2}	20.187 in.^{2}
Wing mean aerodynamic chord	$\bar{c} = 6.01$ in.	6.018 in.
Wing aspect ratio	$A = 2.12$	1.79
Wing taper ratio	$\tau = 0.04$	0.056
Wing dihedral	0°	0°
Wing incidence	0°	0°
Wing geometric twist	0°	0°
Wing leading edge sweepback angle	$\Lambda = 60°$	63.435°

TABLE V (CONT'D)

Max. half-body frontal area	0.925 in.^{2}	1.031
Ratio of max. body frontal area to gross wing area	0.0396	0.05105
Body fineness ratio based on actual body length	10.3	9.88
Body fineness ratio based on extended body length	11.07	12.5

This delta wing model was tested in the N.A.E. 30-inch wind tunnel.

In order to compare the merits of the low wing tail-first configuration with the constant percent chord flap controls it was assumed that the centre of gravity of the tail-first model was moved upstream, to give the same static margin at M = 1.57 (i.e. 15 percent at $C_L = 0$) as was obtained with the flap controlled model with the centre of gravity at 35 percent of the mean aerodynamic chord. This comparison is given in Figure 21 for trim conditions.

The base drag for the constant percent chord flap model was determined as illustrated in Figure 4 and described in Section 4. The base pressure was measured at zero angle of attack and zero flap angle. It was assumed that there is no variation of base pressure with angle of attack and flap angle. The base drag was subtracted from the measured drag.

Due to the higher drag, lower lift-drag ratios were obtained with the tail-first model.

It is evident from Table V that, for a given wing area, the maximum body cross-sectional area, and, therefore, the volume of the tail-first model's body are smaller than those for the flap controlled model. It therefore follows that for models having a comparable body volume the lift-drag ratios obtainable with a tail-first model would have been even smaller than those shown in Figure 21.

Tests on the half body alone of the tail-first model and on a similar body without the fairing at the position of the tail showed that the drag increase due to the fairing was $\Delta C_D = 0.0866$, based on the maximum body cross-section, or $\Delta C_D = 0.00334$ based on the wing area. This ΔC_D equals approximately the difference in C_{D_o} between the tail-first low wing model and the constant percent chord [illegible] have model (Fig. 21). aving ıe tail

However, it should be borne in mind that, in vi[illegible] of the smaller volume of the tail-first model's body (see above), the performance of the tail-first model would have been inferior to that of the flap controlled model having the same body volume even if the extra drag due to the tail fairing were eliminated.

It was desired to compare the performance which might be potentially available with a tail-first model with that of a flap controlled model, both models having the same body shapes and volumes for equal wing areas.

The body of the flap controlled model was tested by the N.A.C.A. (Ref. 2) and showed a drag appreciably lower than that determined for the tail-first model bodies (both with and without tail fairing). It was therefore decided to consider an idealized* tail-first model having a low drag body, identical, both in shape and volume for a given wing area, with that used in the flap controlled model tests.

In order to determine the characteristics of such an idealized tail-first model, the drag of the flap controlled model's body was determined. The NACA data were not used so that a more consistent comparison with the flap-controlled model performance could be made, based on the half-model testing technique, with the same wind tunnel and the same Reynolds number.

---

* In that no provision was made for mounting tail surfaces on the body.

The shape of the body of the flap controlled model, hereafter referred to as the NACA body, was defined by the following equation (Ref. 2).

$$\frac{r}{r_o} = \left[1 - \left(1 - \frac{2x}{l}\right)^2\right]^{\frac{3}{4}}$$

$$\frac{l}{2r_o} = 12.5$$

where l = total reference body length

r_o = maximum radius

r = radius at station x

x = distance from nose

The body was cut off square at $\frac{x}{l} = 0.79$

The drag results obtained for the tail-first half-body, with and without tail fairing and for the NACA half-body are given in Table VI.

TABLE VI BODY DRAG DATA

Model	$(C_D)_{total}$	C_{p_B}	$\frac{S_b}{S_{max.}}$ *	$(C_{D_o})_{base}$	C_{D_o}
Tail-first half-body with tail fairing	0.2805	-0.0535	0.238	0.01275	0.2677
Tail-first half-body without tail fairing	0.1925	-0.048	0.238	0.0114	0.1811
NACA half-body as tested by NAE	0.1525	-0.1075	0.541	0.0581	0.0944 **
NACA half-body as tested by NACA (Ref. 2)	-	-	0.541	-	0.07

* $\frac{S_b}{S_{max.}} = \frac{\text{base area}}{\text{maximum cross section}}$

** Subsequent measurements with another balance and flat nozzle liner showed a higher value. However this does not affect the comparison in this report.

The above values of C_{D_o} are all related to the maximum cross section of the bodies. In all cases the Mach number was 1.57 and the approximate Reynolds number was 5.1×10^6, based on the actual body length. The base pressure was measured at different positions at the base as indicated in Figure 4 (see Section 4). An average value of the so determined base pressures was used to calculate the base pressure coefficient. The variation of the base pressure over the base was within 10 percent of the average value.

The lower base pressure of the N.A.C.A. half-body may have been due to relatively smaller interaction effects between the model wake and the tunnel wall boundary layer, the base area being larger than that of the tail-first model.

In Figure 22 a comparison is made between an idealized low wing tail-first model having an N.A.C.A. half-body and the constant percent chord flap model as measured by the N.A.E. The positions of the centres of gravity of these two models were taken at 21.9 percent and 35 percent of the mean aerodynamic chord respectively, to give the same static margin of 15 percent at $C_L = 0$ and $M = 1.57$. The C_{D_o} value of the body of this tail-first model was taken, $C_{D_o} = 0.0944$, being the value measured by the N.A.E. on a N.A.C.A. half-body. The ratio of the maximum body cross section to wing area was taken, 0.05105, being the same as for the model with the constant percent chord flap.

In contrast with Figure 21, which merely represents the aerodynamic characteristics of the two models for trim conditions as they were obtained from the wind tunnel test data, Figure 22 now represents the characteristics of the two means of longitudinal control on a comparable, if idealized basis, namely same body shape and volume for a given wing area.

Higher lift-drag ratios are obtainable with the idealized tail-first model. For both configurations however the required tail incidence or flap angle are high for moderate values of the balance lift coefficient.

Since it is usual to present aerodynamic data for a centre of gravity at 25 percent of the mean aerodynamic chord, the above mentioned data for trim conditions, Figure 22, are so given in Figure 23.

Comparison of the two configurations, on the basis of the same centre of gravity position (25 percent mean aerodynamic chord) (Fig. 23) indicates that the performance of an idealized tail-first model is much better than the performance of the model with trailing edge flap controls.

7. CONCLUSIONS

With the centre of gravity location at 30.9 percent of the mean aerodynamic chord and at M = 1.57 the tail-first low wing configuration can be trimmed up to lift coefficient of about 0.7 with a tail incidence of 10 degrees. The high wing configuration can be trimmed up to C_L = 0.4 with 10 degrees tail incidence. The static margin however, is about 6.5 percent, which indicates that the configuration is probably unstable subsonically.

The effects of the tail on the wing are relatively small. However, due to the tail fairing the minimum drag is high compared to a configuration without the fairing.

The low wing configuration is a more efficient design than the high wing configuration.

Comparison with a delta wing model having a 25 percent constant percent chord flap at the trailing edge, indicates that higher lift-drag ratios can be obtained with the tail-first configuration. However in both cases the required angles of flap deflection or tail incidence, are high for moderate lift coefficients.

Comparison with a delta wing model having 25 percent constant percent chord trailing edge controls and a slightly larger body volume for a given wing area indicated that for both configurations approximately the same lift-drag ratios were obtainable in trimmed conditions and large control surface deflections were required.

A further comparison was made with an idealized tail-first configuration having the same body as that of the flap-controlled model. Compared with the latter, the idealized tail-first configuration showed larger (by about 20 percent) lift-drag ratios in trimmed conditions, with similar deflections of controls.

8. REFERENCES

1. Lukasiewicz, J.
Stewart, J.D.
LaBerge, J.G.
Half-model tests of two small aspect ratio delta wings at subsonic, transonic, and supersonic speeds.
NAE Laboratory Report LR-92, January, 1954.

2. Heitmeyer, J.C.
Lift, drag and pitching moment of low-aspect-ratio wings at subsonic and supersonic speeds - body of revolution.
NACA RM A51H22, October, 1951.

/LES

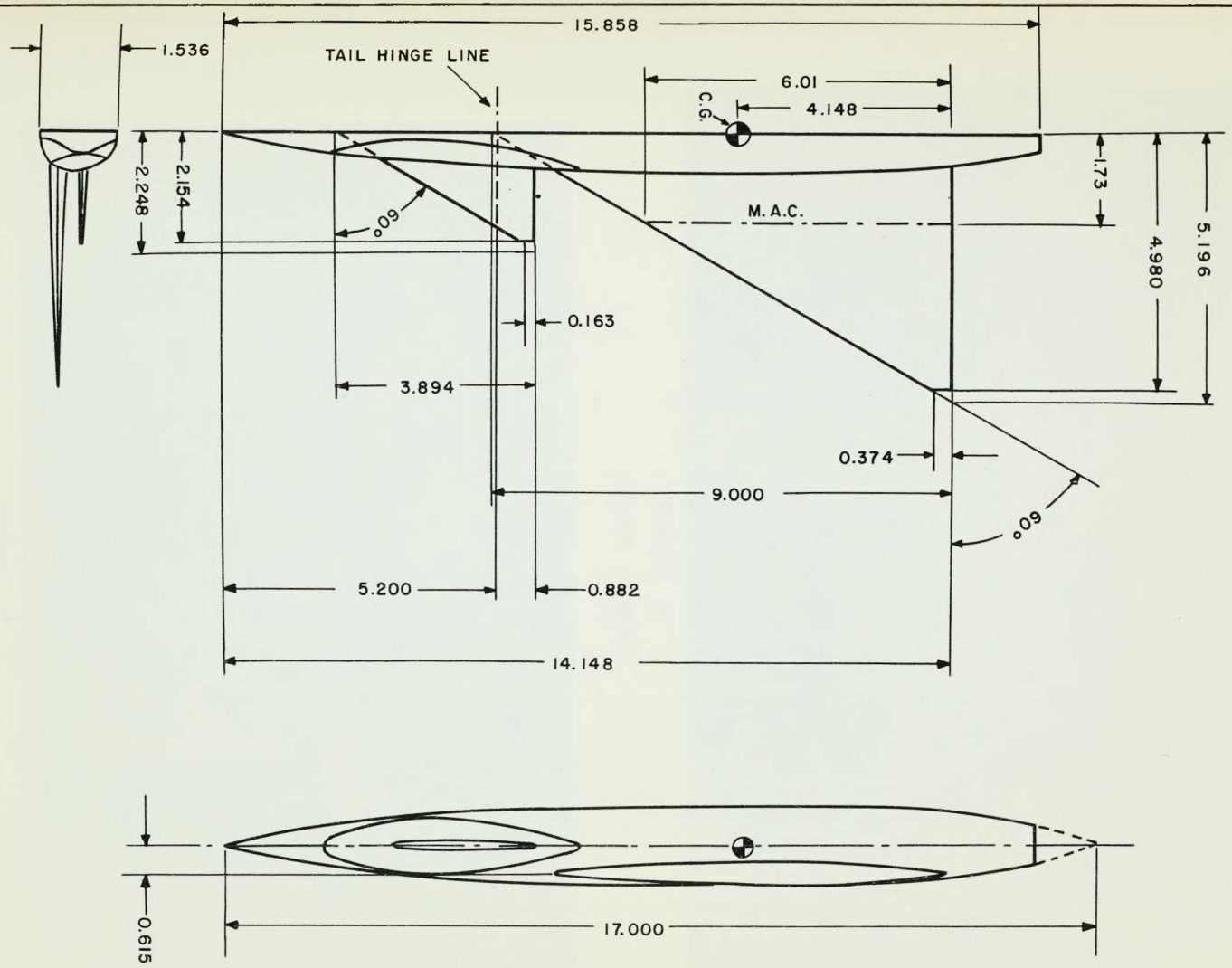

DIMENSIONS IN INCHES

GEOMETRIC PROPERTIES OF TAIL-FIRST MODEL

FIG. 1
LR-116

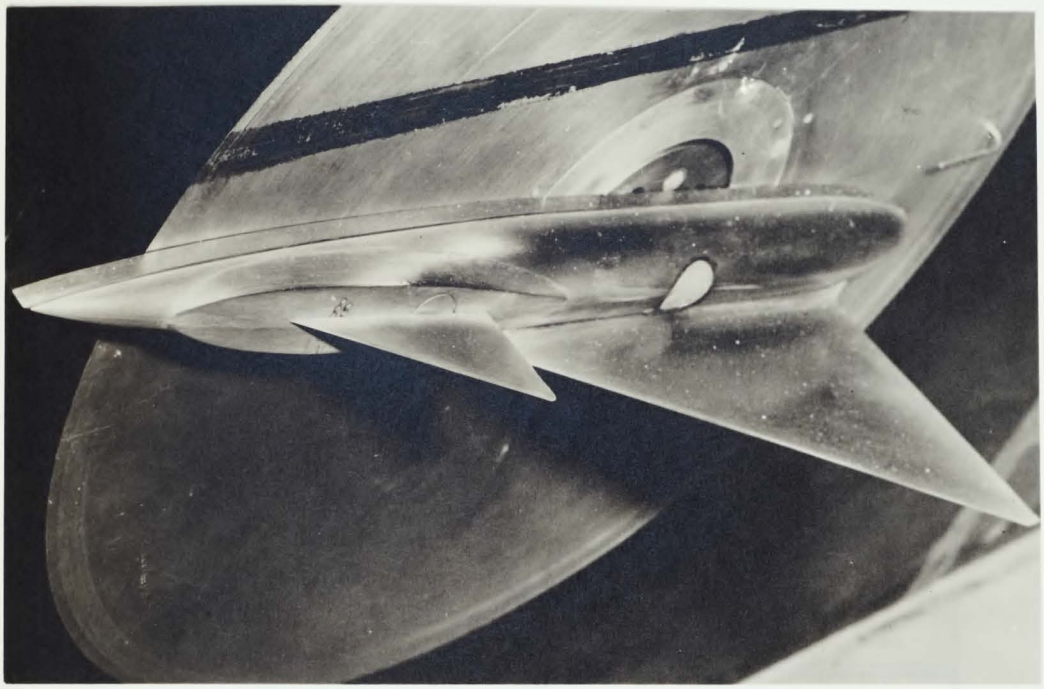

FIGURE 2

FRONT VIEW

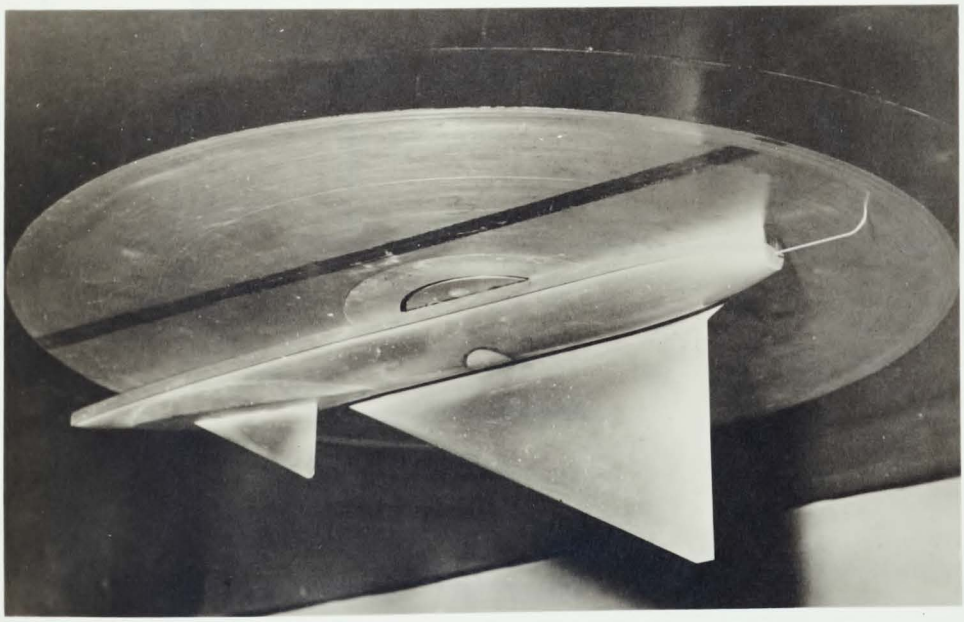

FIGURE 3

REAR VIEW

PHOTOGRAPHS OF MODEL MOUNTED IN WIND TUNNEL

FIG. 4
LR—116

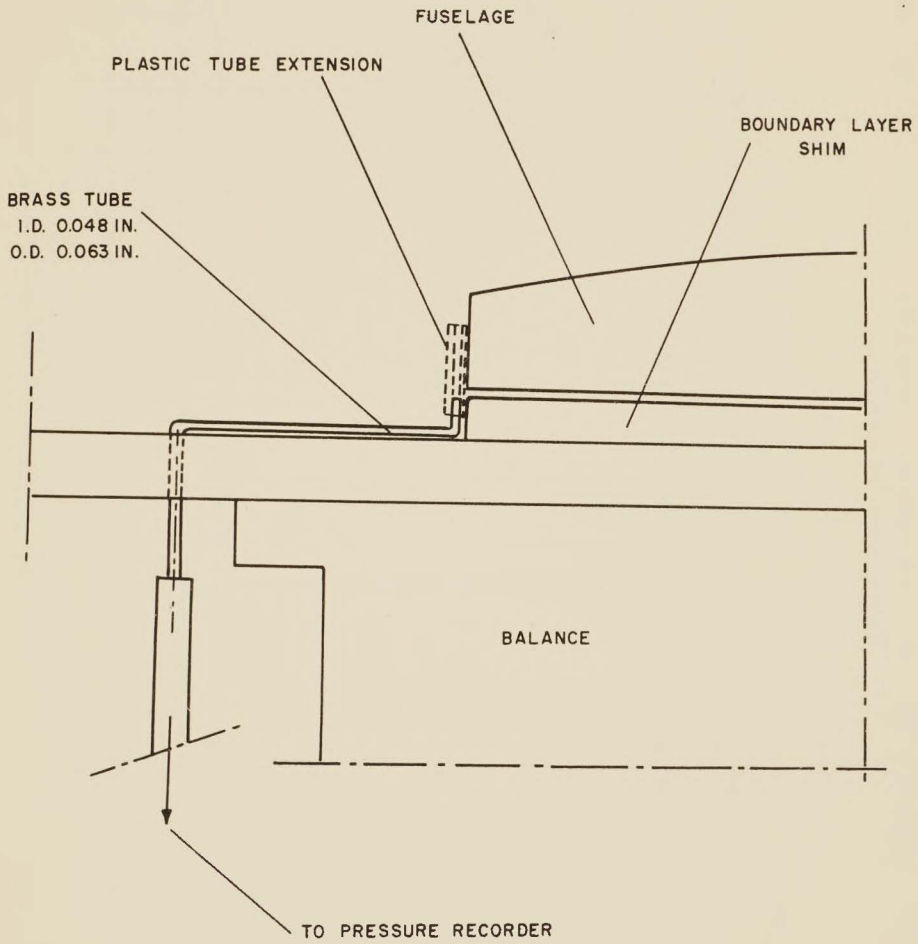

METHOD OF BASE PRESSURE MEASUREMENT

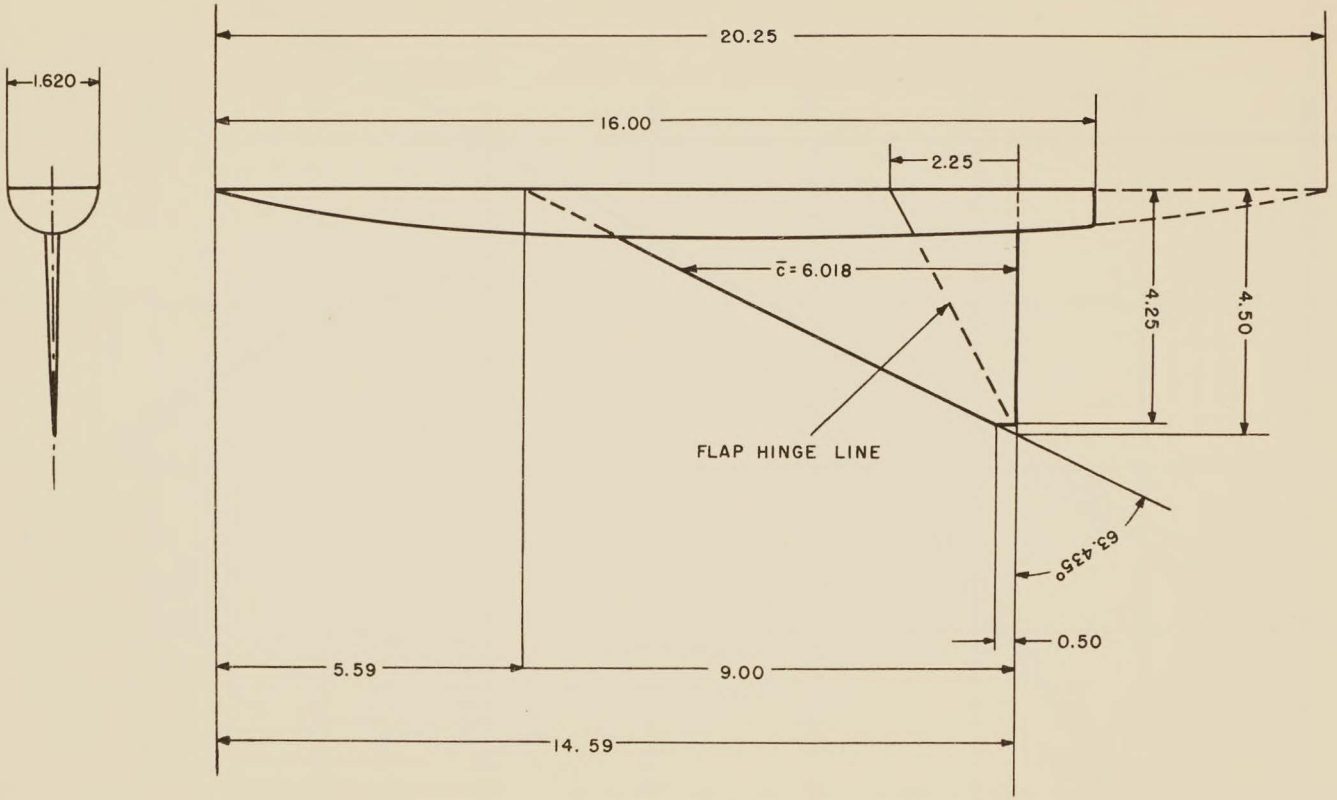

DIMENSIONS IN INCHES

GEOMETRIC PROPERTIES OF CONSTANT PERCENT CHORD FLAP MODEL

FIG. 5
LR-116

FIG. 6
LR-116

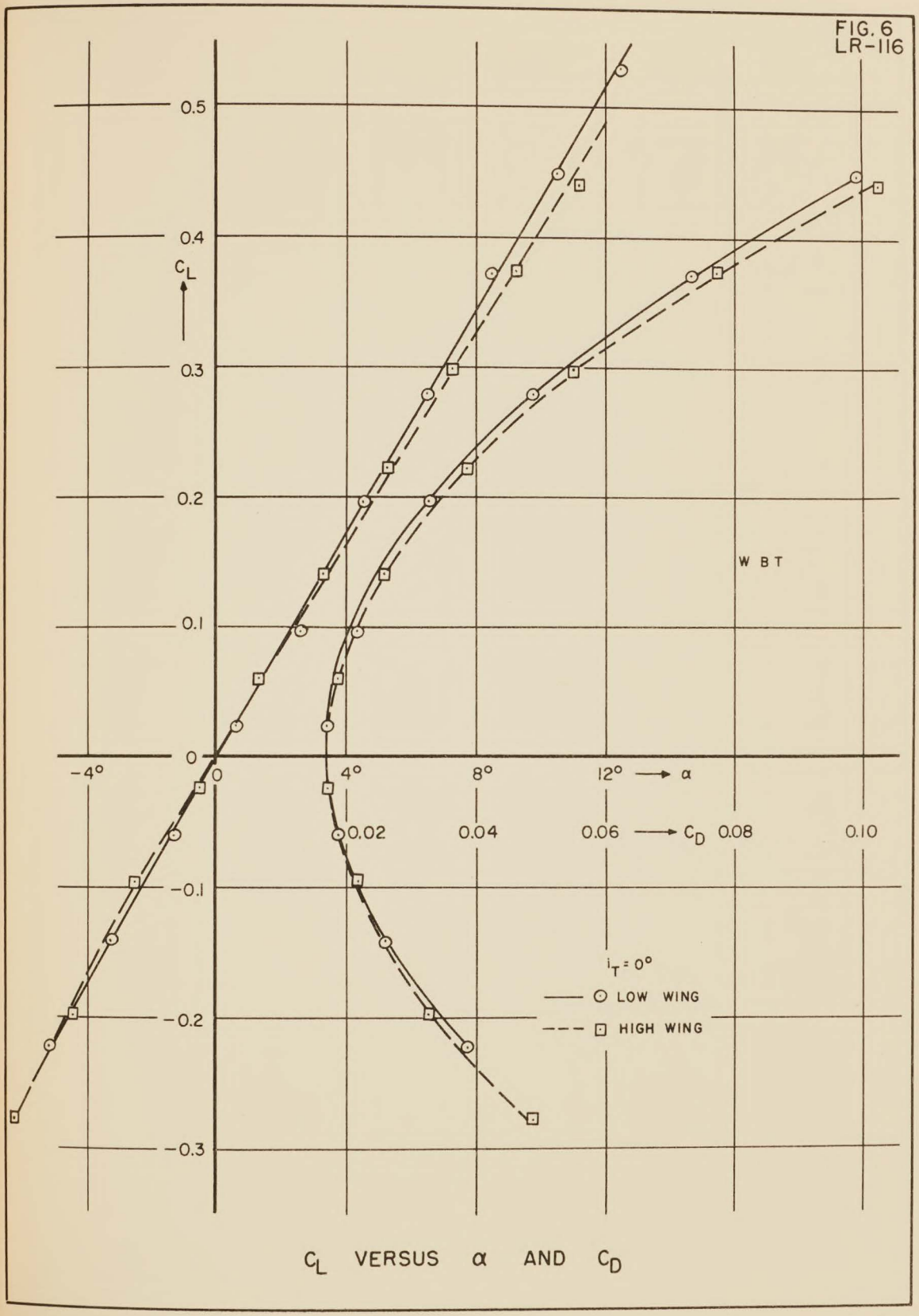

C_L VERSUS α AND C_D

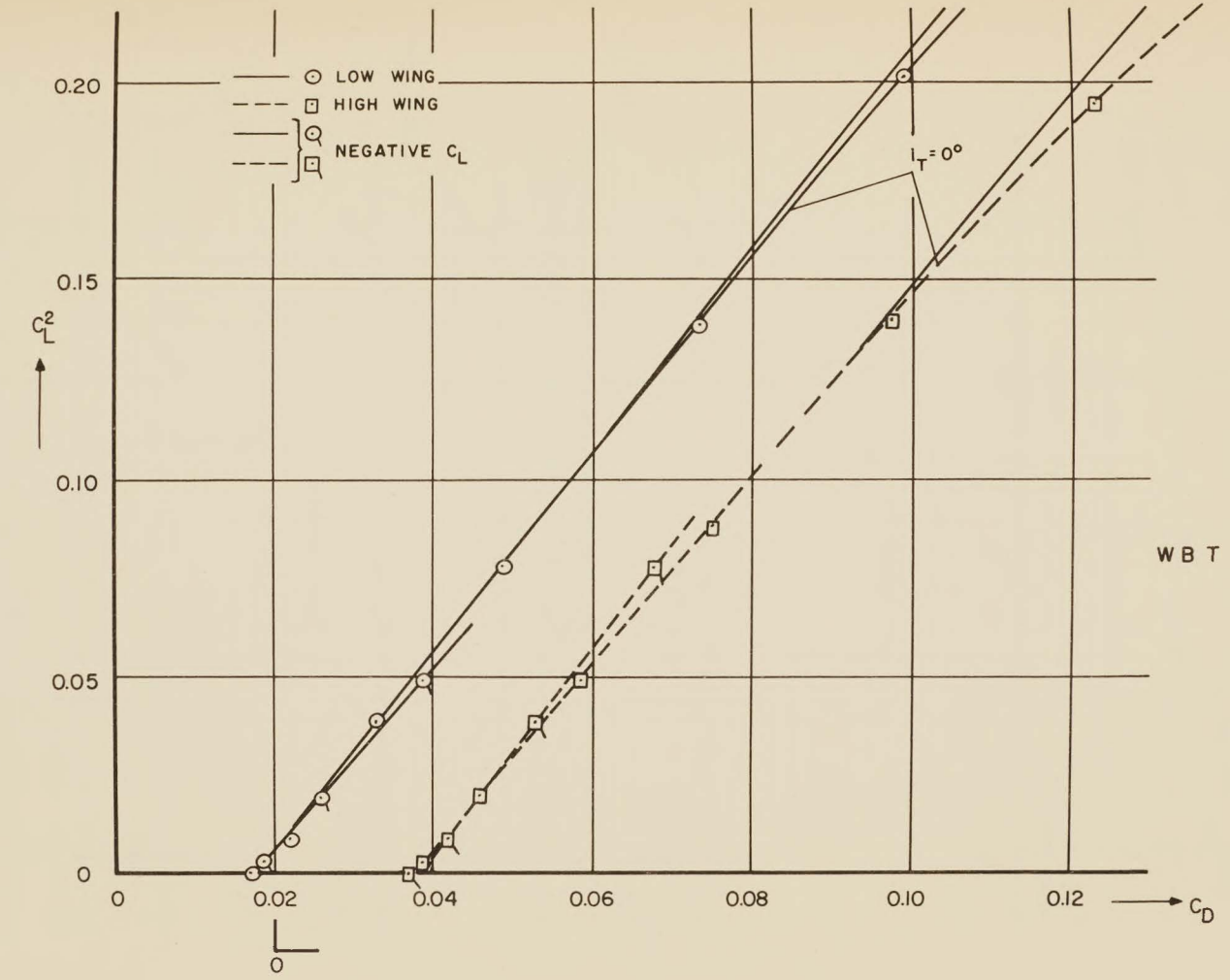

C_L^2 VERSUS C_D

FIG. 10
LR-116

FIG. 14-16
LR-116

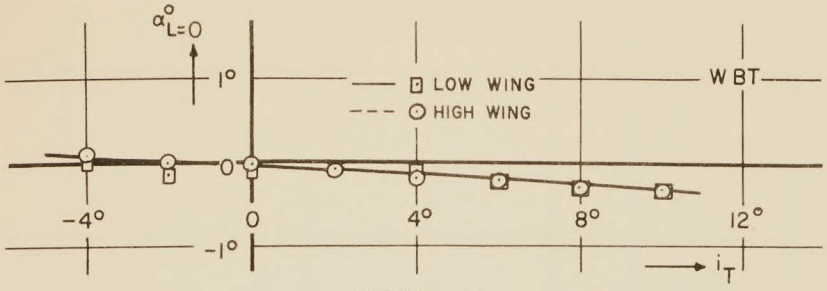

FIGURE 14

$\alpha_{L=0}$ VERSUS i_T

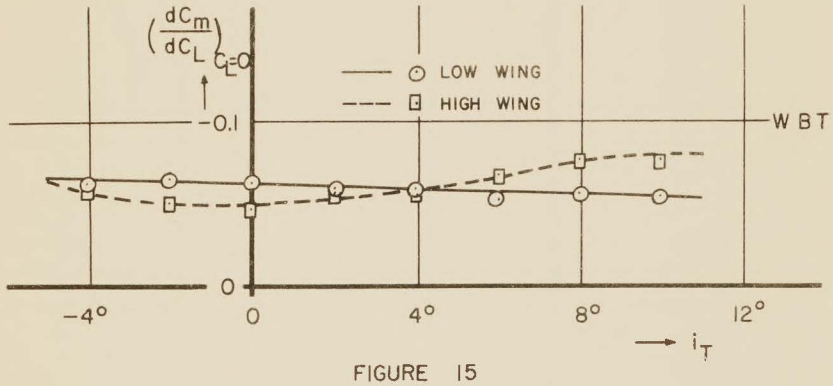

FIGURE 15

$\left(\frac{dC_m}{dC_L}\right)_{C_L=0}$ VERSUS i_T

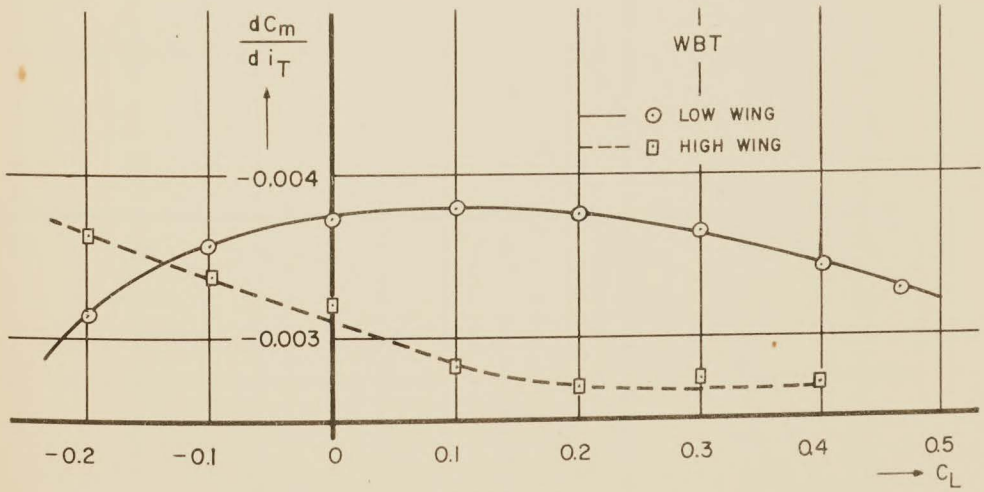

FIGURE 16

$\frac{dC_m}{di_T}$ VERSUS C_L

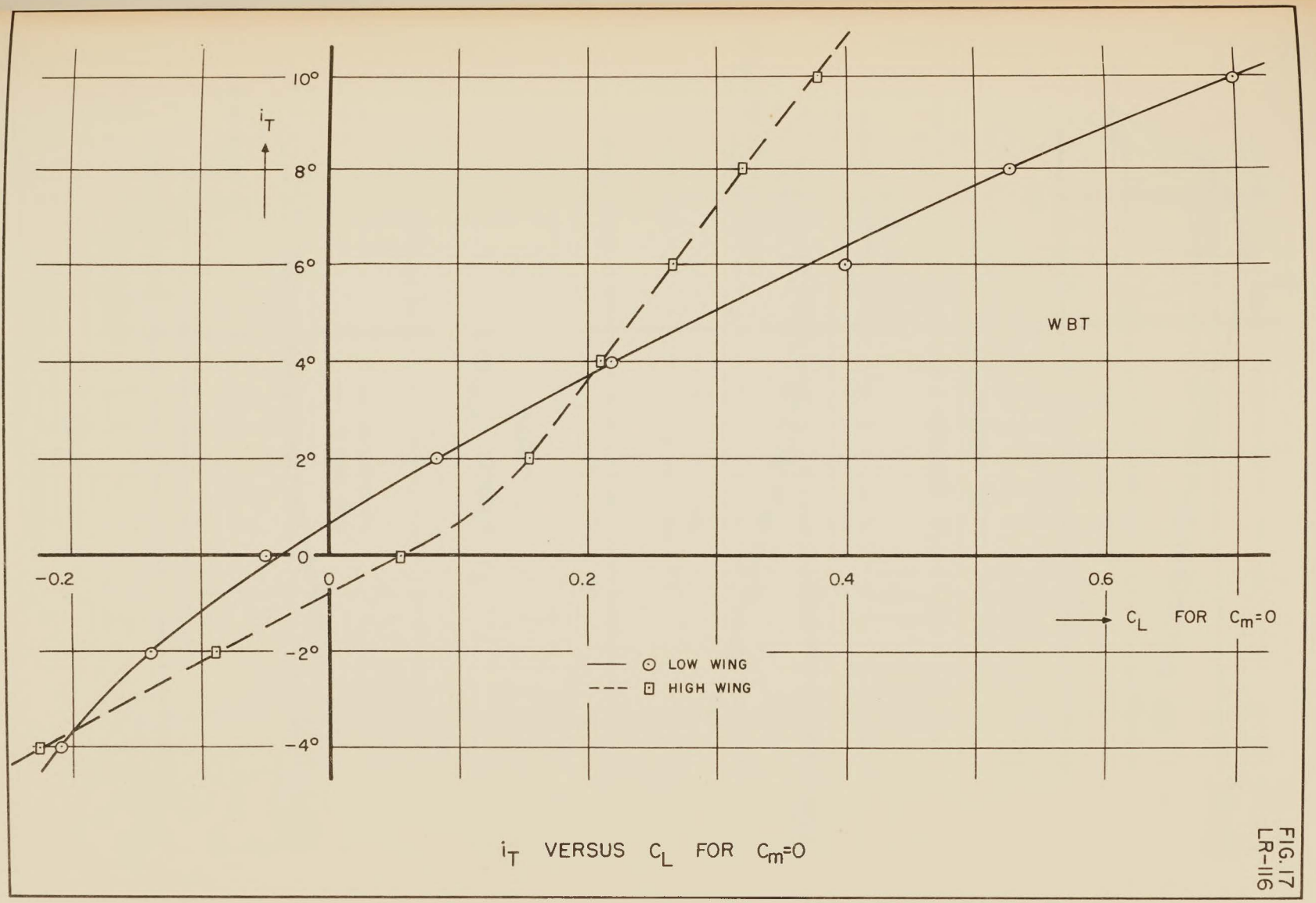

i_T VERSUS C_L FOR C_m=0

FIG. 17
LR-116

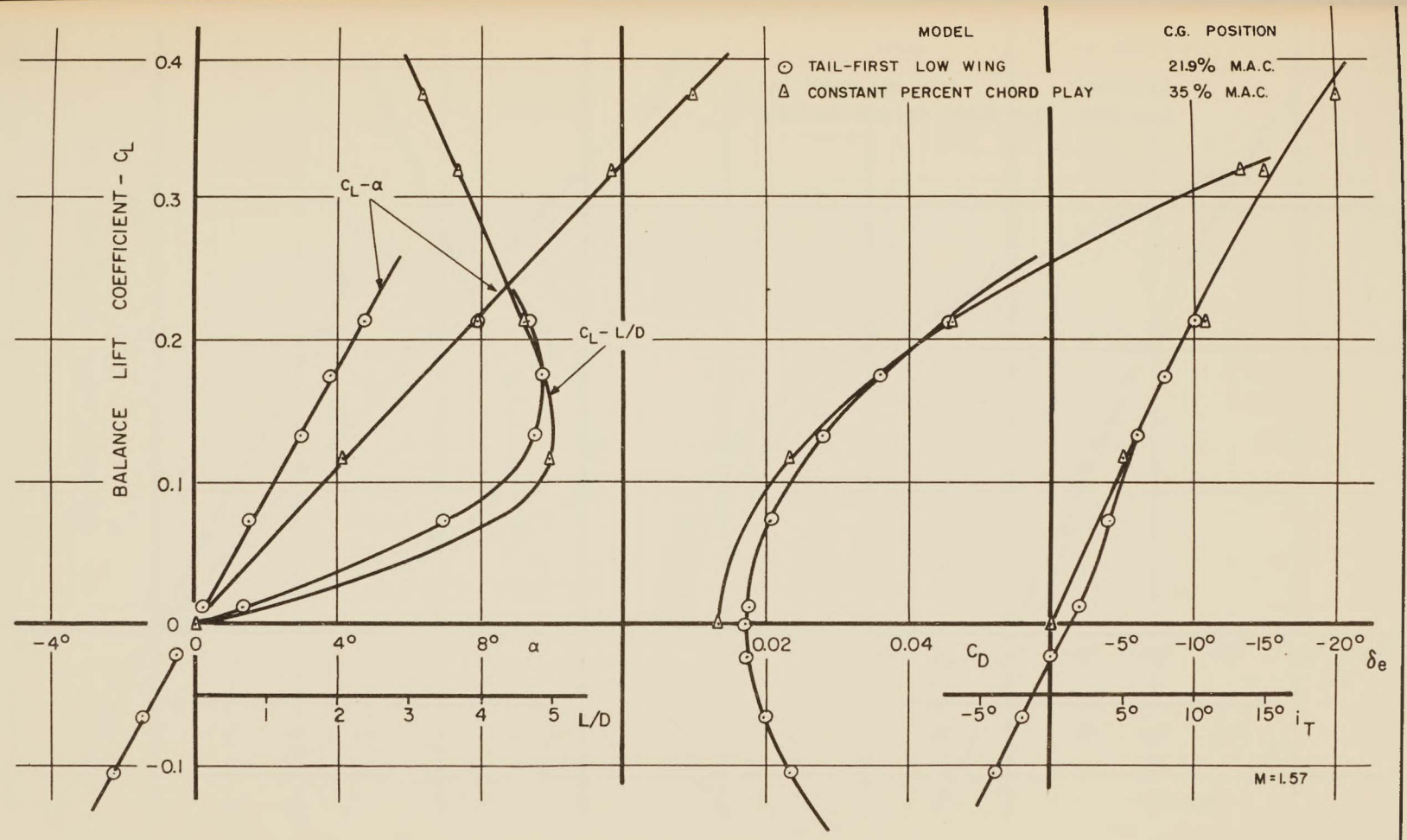

COMPARISON OF TAIL-FIRST MODEL WITH TRAILING EDGE FLAP MODEL

FIG. 21
LR-116

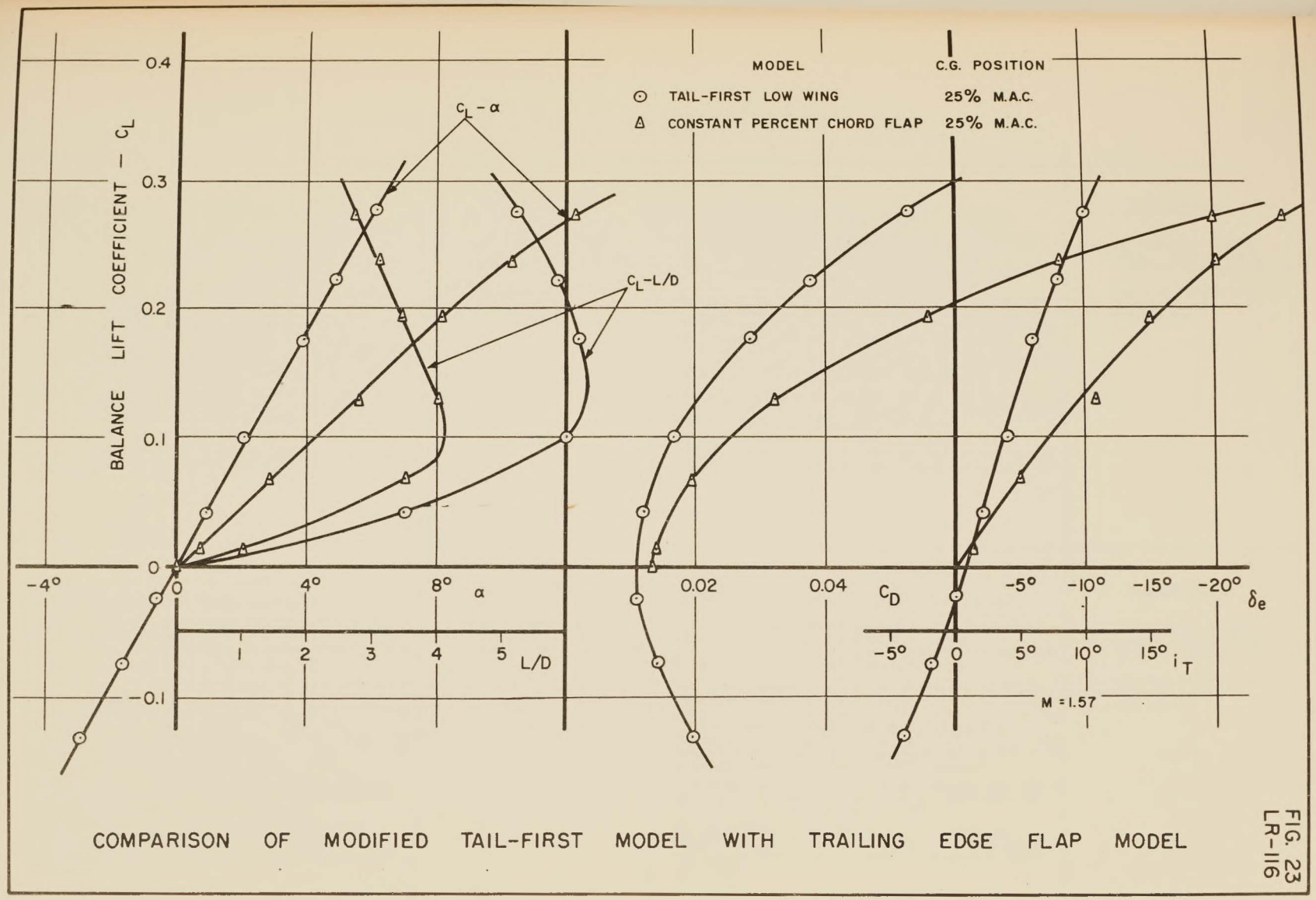

COMPARISON OF MODIFIED TAIL-FIRST MODEL WITH TRAILING EDGE FLAP MODEL

FIG. 23
LR-116